Electromagnetic form factors of the neutron

Hartmut Schmieden

Institut für Kernphysik, Johannes Gutenberg - Universität, 55099 Mainz, Germany

Abstract. Elastic form factors provide information about the charge and current distribution inside proton and neutron. Recent coincidence experiments significantly improved our knowledge of both the electric and magnetic neutron form factors. The results from the $^3\vec{\mathrm{He}}(\vec{e},e'n)$, $\vec{D}(\vec{e},e'n)$ and $D(\vec{e},e'\vec{n})$ double polarization experiments indicate that the neutron electric form factor is almost a factor of two larger than previously assumed from $D(e,e')$ elastic scattering.

INTRODUCTION

The internal structure of the nucleon at very high energies is currently understood in terms of quarks and gluons, and described by perturbative QCD. However, at distances of the size of the nucleon and corresponding momentum transfers of about 1 GeV the strong coupling diverges. Therefore, perturbative methods completely fail to understand the variety of low energy phenomena of the nucleon such as anomalous magnetic moments, polarizabilities or radii.

The elastic form factors parameterize the ability of the composite nucleon to incorporate a momentum transfer, $\vec{q}$, coherently, i.e. without excitation and particle emission. They are related to the distribution of charge and currents and therefore of fundamental importance for the understanding of nucleon structure.

Since R. Hofstadter's pioneering experiments elastic electron scattering has become a unique tool for the investigation of the electromagnetic structure of the nucleon. In the simplest approximation, it is characterized by the exchange of one virtual photon, which transfers the momentum $\vec{q}$ and the energy ω. Electron scattering covers the spacelike region, because the squared four-momentum transfer, $q^2 = \omega^2 - \vec{q}^{\,2}$, is always negative. It is therefore usually expressed by the positive quantity $Q^2 = -q^2 > 0$. The timelike region, where $Q^2 < 0$, can be accessed through electron-positron annihilation into a pair of proton and anti-proton [1] or neutron and anti-neutron [2].

In elastic electron-nucleon scattering the charge-current density of the nucleon can be written in the form [3]:

$$\bar{N}\Gamma_\mu N = \bar{N}\left[\gamma_\mu F_1(Q^2) + \frac{i\sigma_{\mu\nu}q^\nu}{2m_N}\kappa F_2(Q^2)\right]N. \tag{1}$$

The *Dirac* form factor, $F_1(Q^2)$, modifies the vector current of charge and normal magnetic moment. Additionally, the *Pauli* form factor, $F_2(Q^2)$, parameterizes the effect of the anomalous magnetic moment, κ, as motivated by the Gordon decomposition of the electromagnetic current. Linear combinations of F_1 and F_2 constitute the electric and magnetic *Sachs* form factors [4]

$$G_E^{n,p}(Q^2) = F_1^{n,p}(Q^2) - \tau\kappa_{n,p}F_2^{n,p}(Q^2) \tag{2}$$

$$G_M^{n,p}(Q^2) = F_1^{n,p}(Q^2) + \kappa_{n,p}F_2^{n,p}(Q^2), \tag{3}$$

where $\tau = Q^2/4m_N^2$ is a dimensionless measure of the squared four-momentum transfer in units of the nucleon rest mass, m_N. These form factors in the static limit, $Q^2 \to 0$, correspond to the total charge and magnetic moment of protons and neutrons:

$$G_E^{n,p}(Q^2 \to 0) = 0,\ 1 \tag{4}$$

$$G_M^{n,p}(Q^2 \to 0) = -1.91,\ 2.79 \tag{5}$$

In the particular reference frame with vanishing energy transfer, the *Breit* frame, G_E and G_M are interpreted as the Fourier transforms of the corresponding distributions of charge and magnetism. The interpretation of G_E^n in terms of the intrinsic charge distribution was recently discussed again [5, 6, 7, 8].

With these Sachs form factors the cross section for elastic electron-nucleon scattering can be written in the famous *Rosenbluth* form,

$$\frac{d\sigma}{d\Omega} = \left(\frac{d\sigma}{d\Omega}\right)_{\text{Mott}} \cdot \left(\frac{G_E^2 + \tau G_M^2}{1+\tau} + 2\tau G_M^2 \tan^2\frac{\vartheta_e}{2}\right), \tag{6}$$

where $\left(\frac{d\sigma}{d\Omega}\right)_{\text{Mott}}$ is the Mott cross section for electron scattering off a pointlike spin-$\frac{1}{2}$ object and ϑ_e denotes the electron scattering angle. Due to their different angular weights in Eq.6, G_E and G_M can be experimentally separated at constant Q^2.

This method of Rosenbluth-separation has been used in elastic electron-proton scattering [9, 10] to determine G_E^p and G_M^p up to $Q^2 \simeq 9\,(\text{GeV/c})^2$. At higher Q^2 up to $30\,(\text{GeV/c})^2$, G_M^p dominates the cross section and has thus been determined directly [11]. The result was that G_E^p approximately follows the so-called dipole form,

$$\begin{aligned} G_E^p &\simeq G_D = \left(1 + \frac{Q^2}{0.71\,(\text{GeV/c})^2}\right)^{-2}, \qquad \text{and} \\ G_M^p &\simeq \mu_p G_D \end{aligned} \tag{7}$$

scales with its magnetic moment. However, recent results [12] from measurements of the ratio of G_E^p/G_M^p in double polarized elastic scattering, $p(\vec{e},e'\vec{p})$, show with high statistical precision for G_E^p above $Q^2 \simeq 1.5\,(\text{GeV/c})^2$ a substantial faster decrease with momentum transfer than G_M^p. This had already been indicated by older low statistics measurements [13, 14] and is now confirmed by new, still preliminary, double polarization data [15] where this trend continues up to the highest measured momentum transfer of $Q^2 = 5.6\,(\text{GeV/c})^2$.

Generally, the measurement of the neutron form factors raises more difficulties, because there is no free neutron target available which is suited for electron scattering experiments. The best possible approximation of free electron-neutron scattering is quasifree scattering off the lightest nuclei. In $D(e,e')$ single arm experiments the dominating proton contribution has to be subtracted, with corresponding large uncertainties [16]. A Rosenbluth-separation has nevertheless been achieved [17] up to $Q^2 = 4\,(\text{GeV/c})^2$. At low Q^2 nuclear and final state interaction effects are well enough under control [18] to permit an extraction of G_M^n from inclusive quasi-elastic $^3\vec{\text{He}}(\vec{e},e')$ scattering with polarized beam and polarized target [19, 20, 21]. $D(e,e'n)$ coincidence experiments allow the explicit tagging of electron-neutron scattering [14, 22, 23, 24, 25, 26]. The influence of binding effects can be minimized through the simultaneous measurement of the $D(e,e'p)$ reaction. Similar to G_M^p, the neutron magnetic form factor roughly exhibits the dipole behaviour,

$$G_M^n \simeq \mu_n G_D, \tag{8}$$

too.

The situation concerning the neutron electric form factor, G_E^n, is most unfavourable. It must vanish in the static limit, $G_E^n(Q^2 \to 0) = 0$, due to the zero charge of the neutron. The smallness of $(G_E^n)^2$ compared to $\tau(G_M^n)^2$ makes a Rosenbluth decomposition according to Eq.6 very difficult. Due to the corresponding large errors in the small quantity the extracted values for G_E^n are compatible with zero [14, 17]. Therefore, in the momentum transfer range $Q^2 < 1\,(\text{GeV/c})^2$ the most precise data came from *elastic* electron-deuteron scattering [27, 28], where the structure function $A(Q^2)$ depends on the isoscalar form factor $(G_E^p + G_E^n)^2$ and thus provides a higher sensitivity to G_E^n through its interference with the large G_E^p. However, the necessary unfolding of the deuteron wavefunction introduces a substantial model dependence in the extracted neutron electric form factor. This can be overcome by exclusive $(e,e'n)$ double polarization experiments with polarized beam and either polarized target or recoil polarimetry.

RECENT G_M^N EXPERIMENTS

Precise determinations of G_M^n come from unpolarized coincidence experiments at Bates [22], NIKHEF [23], ELSA [24], and MAMI [25, 26]. Except the Bates experiment, which measured the absolute $D(e,e'n)$ cross section, these experiments determined G_M^n from the ratio $R = \frac{\sigma(e,e'n)}{\sigma(e,e'p)}$ of quasifree neutron over proton cross sections off the deuteron with simultaneous neutron/proton detection in one single hadron detector. In this ratio nuclear binding effects cancel

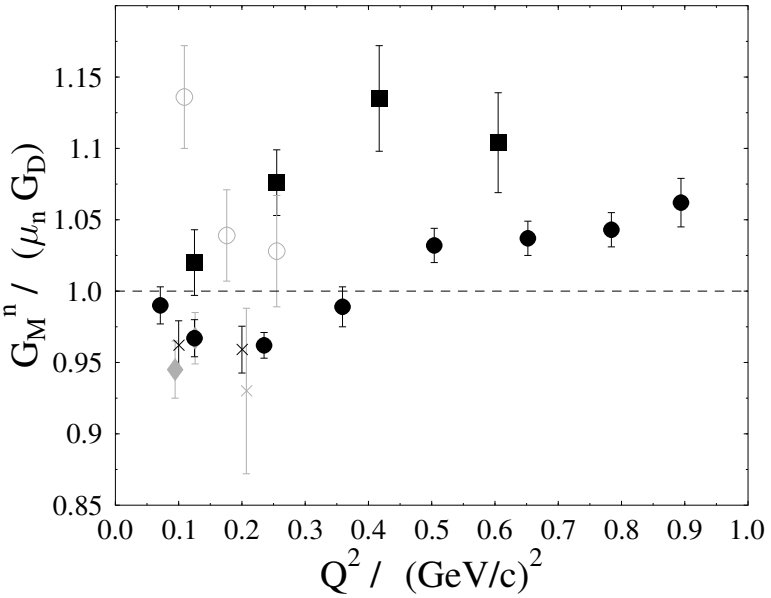

FIGURE 1. Results of recent G_M^n experiments. Gao et al. [19, 20] (grey cross) and Xu et al. [21] (black crosses) exploited the $^3\vec{H}e(\vec{e},e')$ cross section asymmetry. The open circles are the result of the D$(e,e'n)$ experiment of Markowitz et al.[22]. The ELSA [24] (full squares), NIKHEF [23] (grey diamonds) and MAMI [25, 26] (full circles) measurements made use of the ratio method as described in the text.

to a large extent. Moreover, this method is also experimentally insensitive to luminosity fluctuations and detector acceptancies.

Nevertheless, detailed control of the hadron detectors absolute detection efficiency for protons and, particularly, neutrons is essential. The setups of the various experiments have been very similar with the electrons detected in a magnetic spectrometer and coincident n/p-detection in a well shielded plastic or mineral oil scintillator telescope. However, different approaches have been used to determine the absolute neutron detection efficiency. For the Bates and ELSA measurements "in situ" methods were chosen with a bremsstrahlung radiator postioned in front of the experimental target in order to exploit the $D(\gamma,p)n$ or $p(\gamma,\pi^+)n$ reactions, respectively, to tag neutrons in the telescope. In contrast, the hadron detectors which were used at MAMI and NIKHEF were calibrated at the PSI neutron beam in a kinematically complete $p(n,p)n$ experiment. This method relies on the good control and portability of the effective detector thresholds.

Figure 1 shows a comparison of the recent results from Bates [19, 20, 22], ELSA [24], JLab [21], NIKHEF [23], and MAMI [25, 26]. Despite the individual errors of down to 2 %, the MAMI data are approximatly 10 - 15 % below the ELSA ones. The probable origin of this discrepancy is the absolute neutron detection efficiency calibration. In this respect, the possible impact of un-tagged electroproduction events has been discussed for the in situ method [29, 30].

The measurement of the transverse asymmetry $A_{T'}$ from inclusive quasi-elasic $^3\vec{\mathrm{H}}e(\vec{e},e')$ scattering provides an alternative method for the extraction of G_M^n, which is completely independent of efficiency calibrations [19, 20, 21]. However, full Fadeev calculations are required with inclusion of final state interaction and meson exchange currents. Those are currently available for $Q^2 = 0.1$ and $0.2\,(\mathrm{GeV/c})^2$ [18, 21]. The extracted values of G_M^n coincide with the unpolarized measurements of Anklin et al. [23, 25] and Kubon et al.[26].

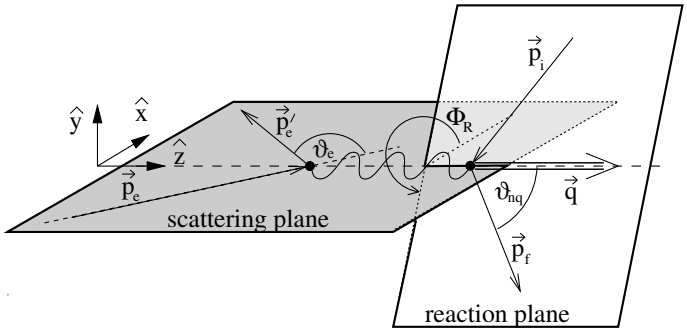

FIGURE 2. Kinematics of the quasifree $n(\vec{e},e'\vec{n})$ reaction with definition of the relevant coordinate frames.

G_E^N DOUBLE POLARIZATION EXPERIMENTS

Double polarization observables in exclusive quasi-free electron-deuteron scattering with longitudinally polarized electrons offer high sensitivity to G_E^n, due to an interference with the large G_M^n, combined with negligible dependence on the deuteron wavefunction [31]. For the ideal case of free electron-neutron scattering, $n(\vec{e},e'\vec{n})$, Arnold, Carlson and Gross [32] obtained for the components of the recoil polarization

$$P_x = -P_e \frac{\sqrt{2\tau\varepsilon(1-\varepsilon)}G_E^n G_M^n}{\varepsilon(G_E^n)^2+\tau(G_M^n)^2} \tag{9}$$

$$P_y = 0 \tag{10}$$

$$P_z = P_e \frac{\tau\sqrt{1-\varepsilon^2}(G_M^n)^2}{\varepsilon(G_E^n)^2+\tau(G_M^n)^2}, \tag{11}$$

where $\hat{x}$ is in the electron scattering plane perpendicular to the direction of the momentum transfer, $\hat{y}$ is normal to the scattering plane, and $\hat{z}$ points into the direction of the momentum transfer, $\vec{q}$ (compare Fig.2). $\varepsilon = (1+\frac{2|\vec{q}|^2}{Q^2}\tan^2\frac{\vartheta_e}{2})^{-1}$ is the photon polarization parameter and P_e denotes the longitudinal polarization of the electron beam.

In the completely equivalent scattering of longitudinally polarized electrons off a polarized neutron target, $\vec{n}(\vec{e},e'n)$, the cross section asymmetry with regard to reversal of the electron beam polarization is given by

$$A = -P_e \frac{\sqrt{2\tau\varepsilon(1-\varepsilon)}G_E^n G_M^n \cdot \tilde{P}_x + \tau\sqrt{1-\varepsilon^2}(G_M^n)^2 \cdot \tilde{P}_z}{\varepsilon(G_E^n)^2+\tau(G_M^n)^2}, \tag{12}$$

where now $\tilde{P}_{x,z}$ are the components of the initial state neutron polarization. The polarized target neutrons can be provided by polarized $^3\vec{\mathrm{He}}$ [33, 34, 35], where the neutron carries approximately 87 % of the polarization of the nucleus [36], or by vector polarized $^2\vec{D}$ [37, 38]. The measurement of asymmetry ratios yields independence of the absolute degree of the target polarization [39, 37].

Polarized target experiments

First experiments aimed at the extraction of G_E^n from the inclusive quasi-elastic reaction $^3\vec{\mathrm{He}}(\vec{e},e')$. The principle feasability of such kind of experiments was successfully demonstrated, but the statistical accuracy remained unsatis-

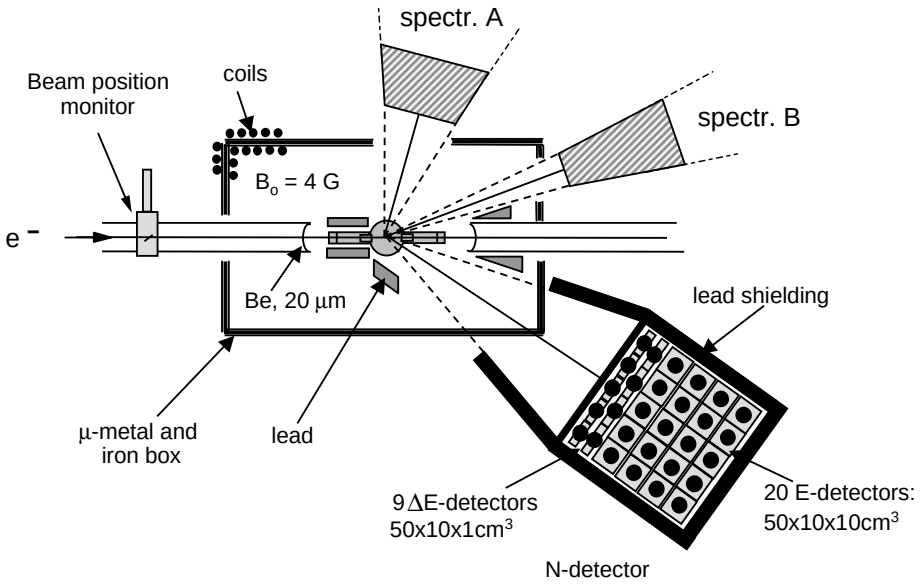

FIGURE 3. Target area of the $^3\vec{\mathrm{He}}(\vec{e},e'n)$ experiment at MAMI. The cell with polarized gas is magnetically shielded against the spectrometers fringe fields.

factory.

The magnetic moment of ^{3}He within 10 % agrees with the free neutron one. Therefore the proton contribution in the measured asymmetries first was expected to be small [36]. Later calculations, however, showed that the remaining impact of the protons on the measured asymmetries is large enough to prohibit a reliable extraction of G_E^n [40].

This problem can be overcome, if the occurence of e-n scattering is explicitly tagged through the detection of the outgoing neutron in coincidence with the scattered electron. Such an exclusive $^3\vec{\mathrm{He}}(\vec{e},e'n)$ experiment was performed for the first time by the A3-collaboration at MAMI [39] at a squared four-momentum transfer of $Q^2 = 0.31\,(\mathrm{GeV/c})^2$. With the detector-setup described in the following section the statistics was improved later on [41]. The most recent experiment at $Q^2 = 0.67\,(\mathrm{GeV/c})^2$ used the 3-spectrometer setup [42] of the A1-collaboration at MAMI [43, 44].

In this experiment the target gas was polarized by metastable optical pumping and subsequently compressed to 6 bars. The glass target cell was then transported in a weak holding field to the experimental place. Under beam conditions an average polarization of 32 % was achieved. The target thickness was 24 mg/cm^2. Thinned down to 25 μm, the beam windows of the glass cell could not stand the 6 bar pressure. Therefore *un*polarized ^{3}He gas of the same pressure was contained between the glass windows and 10 μm thick havar foils, resulting in an empty-target thickness of 27 mg/cm^2.

The relaxation time of approximately one day required twice a day the replacement of the target cell by a freshly polarized one. Quasi-elastic measuremets were performed with target spin aligned perpendicular and parallel to the momentum transfer direction in order to access both the transverse asymmetry, A_x, and the longitudinal asymmetry, A_z. This enabled a measurement of the ratio A_x/A_z, which is directly proportional to G_E^n/G_M^n but independent of both the absolute degrees of beam and target polarization, P_e and P_T, respectively. Furthermore, the product $P_e \cdot P_T$ was monitored through the *elastic* measurement $^3\mathrm{He}(e,e')$ in spectrometer B of the 3-spectrometer setup.

As shown in Fig.3, the quasi-elastically scattered electrons were detected in spectrometer A, the neutrons in coincidence in a dedicated neutron detector provided by the University of Basel. It consisted of four layers of five plastic scintillators of dimensions $50 \times 10 \times 10\,\mathrm{cm}^3$, which were equipped with photomultipliers at both ends. Charged particles could be rejected by means of two layers of 1 cm thick ΔE-counters. The neutron detector was shielded with 2 cm of lead against direct target sight in order to reduce the charged background.

The setup of the JLab Hall C $\vec{D}(\vec{e},e'n)$ experiment in principle is similar [45, 38]. Here the scattered electrons are detected in the HMS spectrometer in coincidence with neutrons in a segmented plastic scintillator. At the required luminosity of $1 \cdot 10^{35}\,\mathrm{cm}^{-2}\mathrm{s}^{-1}$ a 40% polarization of the ND_3 target is achieved by the technique of dynamic nuclear polarization. The deuteron nuclei are polarized by microwave irradiation at temperatures around 1 K in a strong magnetic field of 5 T. In the measurement of A_x this field deflects the incoming electron beam by as much as 4°.

This has to be compensated by a magnetic chicane in order to guarantee horizontal beam at the center of the target. Data have been taken in the Q^2 range between 0.5 and 2 $(\mathrm{GeV/c})^2$, and first results are available at the lowest Q^2 [38].

In contrast to MAMI and JLab, the NIKHEF $\vec{D}(\vec{e},e'n)$ experiment was performed with a vector polarized internal gas target at the AmPS electron storage ring [37]. The scattered electrons were detected in coincidence simultaneously with protons and neutrons. Thus the asymmetry ratio between the $\vec{D}(\vec{e},e'n)$ and $\vec{D}(\vec{e},e'p)$ reactions could be determined.

The $D(\vec{e},e'\vec{n})$ recoil polarization experiment at MAMI

As in the case of polarized targets a pioneering recoil polarization experiment was performed at MIT-Bates [46]. Electrons and neutrons from the $D(\vec{e},e'\vec{n})$ reaction were detected in coincidence and the transverse neutron polarization, P_x, was measured. However, due to the low duty cycle of the Bates linac only modest statistical accuracy could be achieved. Furthermore, the external absolute calibration of the neutron polarimeter's effective analyzing power remained unsatisfactory.

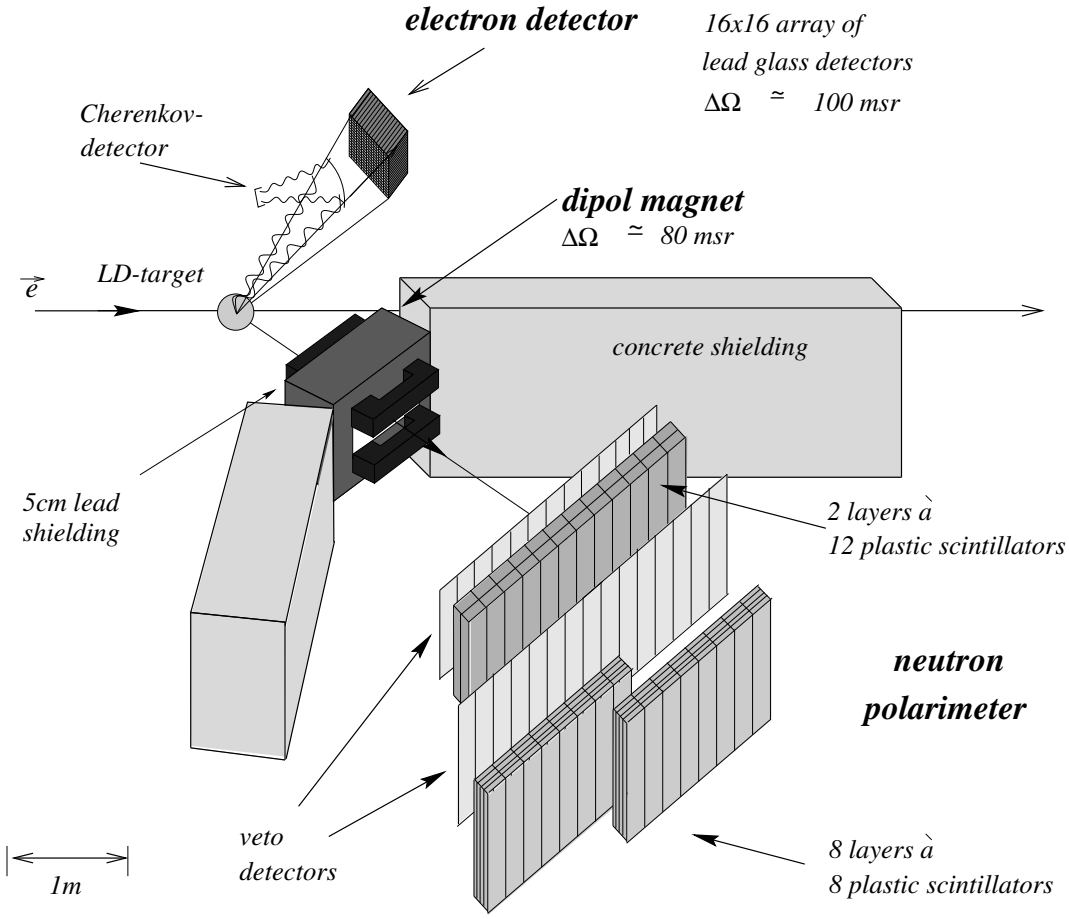

FIGURE 4. Setup of the $D(\vec{e},e'\vec{n})$ experiment at MAMI

The full potential of the recoil polarization method was exploited for the first time at MAMI. Fig.4 shows the experimental setup of this experiment. The longitudinally polarized electron beam ($I \simeq 2.5\,\mu$A, $P_e \simeq 75\,\%$) hit a 5 cm long liquid deuterium target and the scattered electrons were detected in a 256 element lead glass array, which covered a solid angle of $\Delta\Omega \simeq 100$ msr. The energy resolution of $\delta E/E \simeq 25\,\%$ was sufficient to suppress pion production events. Only the electron angles, which were measured with an accuracy of $\delta\vartheta, \delta\phi \simeq 3.5$ mrad entered the event reconstruction, which became kinematically complete through the measurement of the neutrons time-of-flight and hit position in the front plane of the neutron detector.

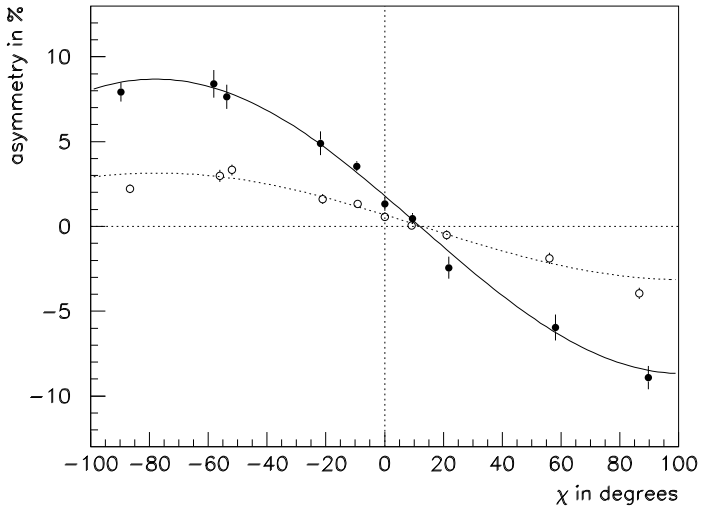

FIGURE 5. Transverse asymmetries as a function of the spin precession angle. The zero crossing is not affected by the different effective analyzing powers obtained by different conditions in the offline analysis (full and open points).

The neutron polarization can be analyzed in the detection process itself [47]. This required a second neutron detection in one of the rear detector planes, which yielded the polar and azimuthal angles, Θ_n' and Φ_n', of the analyzing scattering in the front wall. With the number of events $N^{\pm}(\Phi_n')$ for $\pm$ helicity states of the electron beam the azimuthal asymmetry, $A(\Phi_n')$, was determined through the ratio

$$\frac{1-A(\Phi_n')}{1+A(\Phi_n')} = \sqrt{\frac{N^+(\Phi_n')\cdot N^-(\Phi_n'+\pi)}{N^-(\Phi_n')\cdot N^+(\Phi_n'+\pi)}}, \tag{13}$$

which is insensitive to variations of detector efficiency and luminosity. The extraction of P_x from $A(\Phi_n') = \varepsilon_{\text{eff}} \cdot P_x \cdot \sin\Phi_n'$ requires the calibration of the effective analyzing power, ε_{eff}, of the polarimeter. This, however, varies strongly with the event composition as determined by hardware conditions during data taking and software cuts applied in the offline analysis.

For the first time, the problem of calibration of the effective analyzing power has been avoided by controlled precession of the neutron spins in the field of a dipole magnet in front of the polarimeter [48] (see Fig.4). After precession by the angle χ the transverse neutron polarization behind the magnet, $P_\perp$, is a superposition of x and z components, and likewise is the measured asymmetry:

$$A_\perp = A_x \cos\chi - A_z \sin\chi. \tag{14}$$

In the particular case of the zero crossing, $A_\perp(\chi_0) = 0$, one immediately gets the relation

$$\tan\chi_0 = \frac{A_x}{A_z} = \frac{\varepsilon_{\text{eff}}\cdot P_e \cdot \sqrt{2\tau\varepsilon(1-\varepsilon)}\, G_E^n \cdot G_M^n}{\varepsilon_{\text{eff}}\cdot P_e \cdot \tau\sqrt{1-\varepsilon^2}\,(G_M^n)^2}. \tag{15}$$

Obviously, this ratio is independent of both the degree of electron beam polarization, P_e, and the polarimeter's effective analyzing power. It therefore directly yields G_E^n/G_M^n. Different effective analyzing powers do change the magnitude of the transverse asymmetry, $A_\perp$, but not the zero crossing angle, χ_0 [48]. This is demonstrated in Fig. 5, where $A_\perp$ is plotted for two different cut conditions in the offline analysis (full and open points) as a function of the spin precession angle, χ. The magnitude of the asymmetry is affected but the zero crossing remains unchanged.

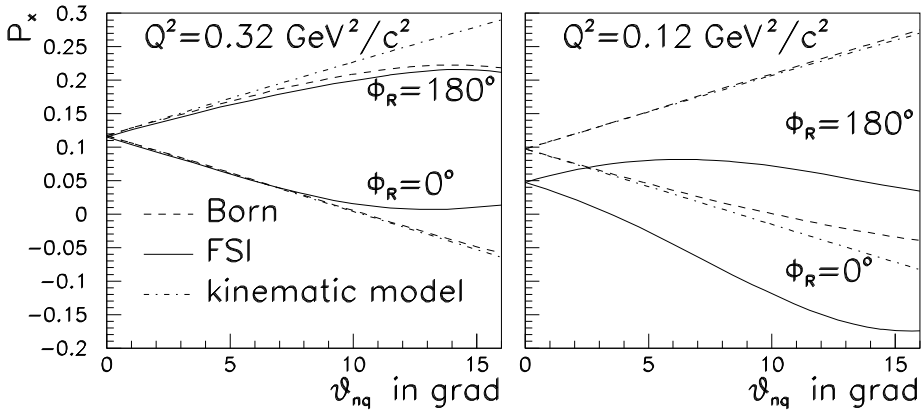

FIGURE 6. The polarization component P_x, calculated for the event population of the $D(\vec{e},e'\vec{n})$ experiment at MAMI, as a function of the angle between the outgoing neutron and the momentum transfer direction, ϑ_{np}, without final state interaction (Born) and with final state interaction (FSI). Left and right parts are for $Q^2 = 0.32\,(\mathrm{GeV/c})^2$ and $Q^2 = 0.12\,(\mathrm{GeV/c})^2$, respectively. The kinematical model takes into account only the proper rotation of quantization axes between neutron rest frame and laboratory frame required by Fermi motion.

Final state interaction

Data have been taken around $Q^2 = 0.32\,(\mathrm{GeV/c})^2$ and $Q^2 = 0.12\,(\mathrm{GeV/c})^2$. According to calculations of H. Arenhövel [49] the effect of final state interaction on P_x – which is dominated by charge exchange of the outgoing nucleons – is almost negligible at the higher momentum transfer. However, due to the small relative energy in the n-p final state, it becomes important at the small Q^2. This is illustrated in Fig.6. P_x, as calculated for the event population of the MAMI experiment [50], is plotted as a function of the angle ϑ_{nq} of the outgoing neutron with respect to $\vec{q}$ for the two extreme situations $\Phi_R = 0$ (left of $\vec{q}$) and $\Phi_R = 180^o$ (right of $\vec{q}$). For $\vartheta_{nq} \leq 10^o$ the general behaviour is well approximated by purely kinematical effects due to Fermi motion and can therefore be understood within a kinematical model [50] (dashed-dotted curves). The effect of final state interaction is exhibited in the difference between the dashed lines (Born calculation, i.e. without FSI) and the full curves, which include FSI. As expected, this difference is very small at $Q^2 = 0.32\,(\mathrm{GeV/c})^2$ (Fig.6, left), but it is roughly 50 % at $Q^2 = 0.12\,(\mathrm{GeV/c})^2$ (Fig.6, right). Despite its size, the required correction of the G_E^n/G_M^n ratio extracted from P_x has only small uncertainties, because it is insensitive to the choice of N-N potential and G_E^n parameterization [49]. Therefore, even at $Q^2 = 0.12\,(\mathrm{GeV/c})^2$ a reliable extraction of G_E^n/G_M^n is possible. The longitudinal neutron polarization, P_z, remains almost unaffected by FSI. The neutron electric form factor, G_E^n, has been extracted from the ratio G_E^n/G_M^n relying on the dipole values for G_M^n (Eq.8).

RESULTS

Fig. 7 gives a summary of the recent double polarization measurements with statistical (inner) and systematical (outer) errors. The recoil polarization experiments are depicted by circles, full for the MAMI results [48, 50] and open for the Bates one [46]. The open squares indicate the NIKHEF [37] and JLab [38] polarized target measurements. The full squares represent the MAMI results for $^3\vec{\mathrm{He}}(\vec{e},e'n)$. For the $^3\vec{H}e$ experiments FSI is expected to be small at $Q^2 = 0.67\,(\mathrm{GeV/c})^2$ [43], due to the large kinetic energy of the ejected neutron. Contrary, at $Q^2 = 0.36\,(\mathrm{GeV/c})^2$ (grey square) [41] first, still incomplete, Fadeev calculations indicate a substantial correction of the $^3\vec{\mathrm{He}}(\vec{e},e'n)$ data point towards larger G_E^n. At the present status of calculation where no meson exchange currents are yet included the central value of the extracted G_E^n is shifted by approximately 50 % [18] (black square). Due to the kinematical reconstruction the average Q^2 is also shifted. Despite the small statistical error, this data point has the largest systematical and theoretical (model) uncertainty, which is not included in the depicted error.

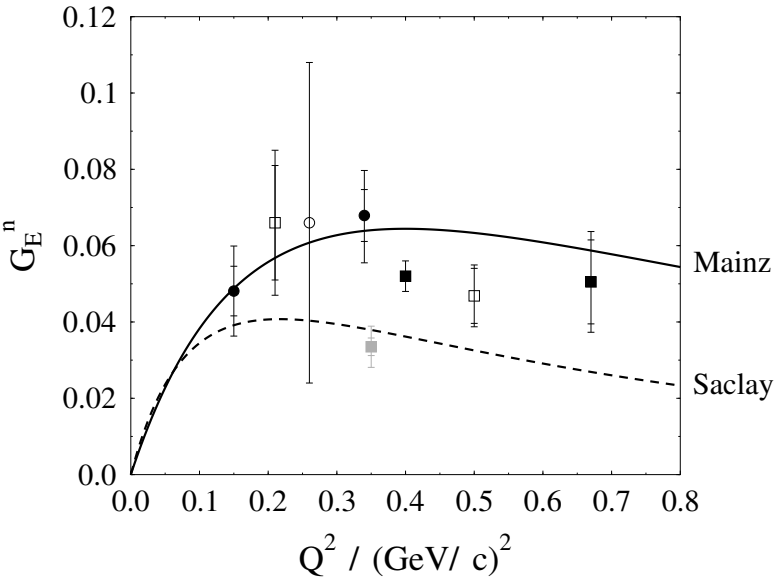

FIGURE 7. Results for G_E^n from the $D(\vec{e},e'\vec{n})$ experiment at MAMI (full circles) [48, 50] along with the $^3\vec{\mathrm{He}}(\vec{e},e'n)$ results from MAMI (full squares) [41, 43], the $D(\vec{e},e'\vec{n})$ result from Bates (open circle) [46], and the $\vec{D}(\vec{e},e'n)$ results from NIKHEF (open square at $Q^2 = 0.2\,(\mathrm{GeV/c})^2$) [37] and JLab (open square at $Q^2 = 0.5\,(\mathrm{GeV/c})^2$) [38]. Except the Bates data point the deuterium results are FSI-corrected. The FSI correction of the $^3\vec{\mathrm{H}}e$ results and the curves are discussed in the text.

Therefore, for a new one parameter fit of

$$G_E^n = -\frac{\mu_n \tau}{1+\eta\tau} \cdot G_D \tag{16}$$

this data point was omitted. Based on the recent MAMI $D(\vec{e},e'\vec{n})$ results of Herberg et al. and Ostrick et al., and the $^3\vec{\mathrm{He}}(\vec{e},e'n)$ result of Rohe et al., the fit yielded $\eta = 3.4$ [50] (full line in Figure 7). Such a fit reproduces within the errors the neutron's measured rms charge radius [51], which is related to the slope of $G_E^n(Q^2 \to 0)$. It lies almost a factor of two above the so far favoured result from elastic $D(e,e')$ scattering, where the Paris potential has been used for the unfolding of the wave function contribution [28] (indicated by the dashed curve in Figure 7).

This causes a significant difference between the respective Fourier transforms, which correspond to the neutron charge distribution in the Breit frame. The full and broken curves in Fig.8 correspond to the Mainz and Saclay parameterizations of G_E^n, respectively.

SUMMARY AND OUTLOOK

Elastic form factors contain information about the distribution of charge and current in the nucleon ground state. Precise proton magnetic form factor data are available up to $Q^2 = 30$ (GeV/c)^2, roughly exhibiting dipole behaviour. Above $Q^2 \simeq 1.5\,(\mathrm{GeV/c})^2$ the proton electric form factor falls significantly faster than the dipole form factor.

The neutron magnetic form factor, G_M^n, could be extracted up to $Q^2 = 4$ (GeV/c)^2 from single arm $D(e,e')$ quasi-elastic scattering. Below $Q^2 = 1$ (GeV/c)^2, recent coincidence experiments allowed a precise determination of G_M^n from the ratio $R = \frac{\sigma(e,e'n)}{\sigma(e,e'p)}$ of quasi-free electron scattering cross sections off the deuteron. Despite their individual statistical errors of only 2 %, two datasets from ELSA and MAMI/NIKHEF differ by as much as 10 - 15 %. This discrepancy presently represents the largest error contribution for the extraction of strange form factors from parity violating $p(\vec{e},e')$ electron scattering [52]. Recent results from $^3\vec{\mathrm{He}}(\vec{e},e'n)$ measurements at $Q^2 \leq 0.2\,(\mathrm{GeV/c})^2$ [20, 21]

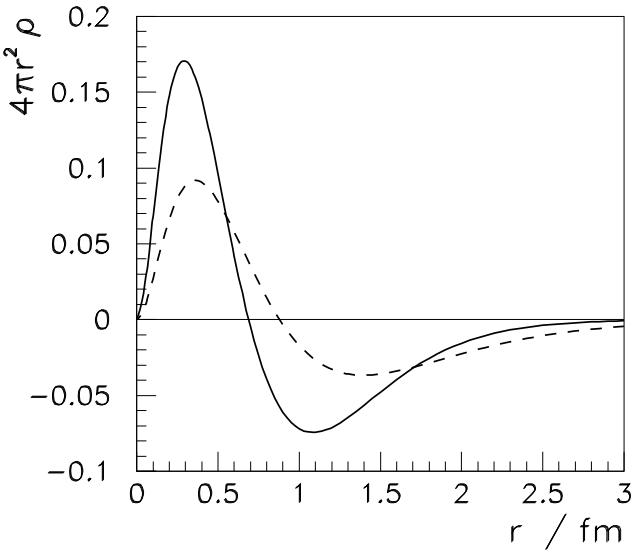

FIGURE 8. Charge density of the neutron in the Breit frame as obtained by Fourier transformation of the Saclay (dashed curve) and Mainz (full curve) G_E^n parameterizations.

tend to prefer the MAMI/NIKHEF dataset. The solution to the discrepancy between the G_M^n datasets is important also as a normalization for the recent double polarization experiments $^3\vec{\mathrm{H}}\mathrm{e}(\vec{e},e'n)$, $\vec{D}(\vec{e},e'n)$ and $D(\vec{e},e'\vec{n})$ at various laboratories, where the neutron electric form factor is extracted from the ratio G_E^n/G_M^n of electric to magnetic neutron form factors.

In the $D(\vec{e},e'\vec{n})$ experiment at MAMI the neutron polarimeter was, for the first time, supplemented by a spin precessing dipole magnet. This technique, which is also adopted for the corresponding JLab experiment, avoids the polarimeter's analyzing power calibration. The influence of final state interaction has been quantitatively evaluated for the $D(\vec{e},e'\vec{n})$ reaction. At the lowest Q^2 a significant FSI correction is required for the extracted G_E^n. After this correction the data are consistently described by a new one parameter fit which lies almost a factor of two above the so far favoured result from elastic electron deuteron scattering. It will be important to continue these G_E^n experiments at larger Q^2.

At JLab and MAMI there are further measurements underway, both with polarized target [45, 53] and recoil polarimetry [54, 55]. These experiments will further exploit the potential of double polarized quasi-elastic electron scattering.

ACKNOWLEDGEMENTS

The MAMI experiments have been performed within the framework of the collaborations A1 and A3 with contributions of institutes of the Universities of Basel, Bonn, Glasgow, Mainz, and Tübingen. H. Arenhövel supplied all the necessary calculations for the FSI correction of the deuteron measurements. The spin precession magnet for the $D(\vec{e},e'\vec{n})$ experiment was provided by the Physikalisches Institut of the University of Bonn. The MAMI experiments are financially supported by the Deutsche Forschungsgemeinschaft (SFB 443).

REFERENCES

1. T.A. Armstrong et al., *Phys. Rev. Lett.* **70**, 1212 (1993), and
   G. Bardin et al., *Nucl. Phys.* B **411**, 3 (1994) and references therein
2. A. Antonelli et al., *Nucl. Phys.* B **517**, 3 (1998)
3. J.D. Bjørken and S.D. Drell, Relativistic quantum mechanics, McGraw-Hill 1964

4. R.G. Sachs, *Phys. Rev.* **126**, 2256 (1962)
5. N. Isgur, *Phys. Rev. Lett.* **83**, 272 (1999)
6. F. Cardarelli and S. Simula, *Phys. Lett.* B **467**, 1 (1999)
7. D.B. Leinweber, A.W. Thomas, and R.D. Young, *Phys. Rev. Lett.* **86**, 5011 (2001)
8. M. Bawin and S.A. Coon, *Nucl. Phys.* A **689**, 475 (2001)
9. P. Bosted et al., *Phys. Rev. Lett.* **68**, 3841 (1992)
10. A.F. Sill et al., *Phys. Rev.* D **48**, 29 (1993)
11. R.G. Arnold et al., *Phys. Rev. Lett.* **57**, 174 (1986)
12. M.K. Jones et al., *Phys. Rev. Lett.* **84**, 1398 (2000)
13. Ch. Berger et al., *Phys. Lett.* B **35**, 87 (1971)
14. W. Bartel et al., *Nucl. Phys.* B **58**, 429 (1973)
15. C.F. Perdrisat, these proceedings
16. for a compilation see I. Sick, Proc. 6^{th} Miniconference on electron scattering, p. 193, NIKHEF 1989
17. A. Lung et al., *Phys. Rev. Lett.* **70**, 718 (1993)
18. J. Golak et al., *Phys. Rev.* C **63**, 034006 (2001)
19. H. Gao et al., *Phys. Rev.* C **50**, R546 (1994)
20. H. Gao, Bates25, Cambridge, MA, AIP Conference Proceedings **520** (1999)
21. W. Xu et al., *Phys. Rev. Lett.* **85**, 2900 (2000)
22. P. Markowitz et al., *Phys. Rev.* C **48**, R5 (1993)
23. H. Anklin et al., *Phys. Lett.* B **336**, 313 (1994)
24. E. Bruins et al., *Phys. Rev. Lett.* **75**, 21 (1995)
25. H. Anklin et al., *Phys. Lett.* B **428**, 248 (1998)
26. G. Kubon et al., nucl-ex/0107016
27. S. Galster et al., *Nucl. Phys.* B **32**, 221 (1971)
28. S. Platchkov et al., *Nucl. Phys.* A **510**, 740 (1990)
29. J. Jourdan et al., *Phys. Rev. Lett.* **79**, 5186 (1997)
30. E. Bruins et al., *Phys. Rev. Lett.* **79**, 5187 (1997)
31. H. Arenhövel, *Phys. Lett.* B **199**, 13 (1987) and *Z. Phys.* A **331**, 509 (1988)
32. R.G. Arnold et al., *Phys. Rev.* C **23**, 363 (1981)
33. G. Eckert et al., *Nucl. Instr. Meth.* A **320**, 53 (1992) and W. Heil et al., *Phys. Lett.* A **201**, 337 (1995)
34. C.E. Woodward et al., *Phys. Rev. Lett.* **65**, 698 (1990)
35. T.E. Chupp et al., *Phys. Rev.* C **45**, 915 (1992)
36. J. Friar, *Phys. Rev.* C **42**, 2310 (1990)
37. I. Passchier et al., *Phys. Rev. Lett.* **82**, 4988 (1999)
38. H. Zhu et al., nucl-ex/0105001
39. M. Meyerhoff et al., *Phys. Lett.* B **327**, 201 (1994)
40. R. Schulze and P. Sauer, *Phys. Rev.* C **48**, 38 (1993)
41. J. Becker et al., *Eur. Phys. J.* A **6**, 329 (1999)
42. K.I. Blomqvist et al., *Nucl. Instr. Meth.* A **403**, 263 (1998)
43. D. Rohe et al., *Phys. Rev. Lett.* **83**, 4257 (1999)
44. J. Bermuth, doctoral thesis, Mainz (in preparation)
45. D. Day et al., JLab proposal E-93-026 (1993)
46. T. Eden et al., *Phys. Rev.* C **50**, R1749 (1994)
47. T.N. Taddeucci et al., *Nucl. Instr. Meth.* A **241**, 448 (1985)
48. M. Ostrick et al., *Phys. Rev. Lett.* **83**, 276 (1999)
49. H. Arenhövel, priv. comm., 1998
50. C. Herberg et al., *Eur. Phys. J.* A **5**, 131 (1999)
51. S. Kopecky et al., *Phys. Rev.* C **56**, 2229 (1997)
52. J. Martino, these proceedings
53. W. Heil et al., approved MAMI proposal A1/4-95 (1995)
54. R. Madey and S. Kowalski et al., approved JLab proposal E93-038 (1993)
55. U. Müller and H. Schmieden et al., approved MAMI proposal A1/2-99 (1999)